JOC The Journal of Organic Chemistry

Article

pubs.acs.org/joc

Intramolecular Halogen Bonding Supported by an Aryldiyne Linker

Danielle L. Widner,[†] Qianwei R. Knauf,[†] Mark T. Merucci,[†] Thomas R. Fritz,[†] Jon S. Sauer,[†] Erin D. Speetzen,[†] Eric Bosch,[‡] and Nathan P. Bowling*[,†]

[†]Department of Chemistry, University of Wisconsin-Stevens Point, 2001 Fourth Avenue, Stevens Point, Wisconsin 54481, United States

[‡]Department of Chemistry, Missouri State University, 901 S. National Avenue, Springfield, Missouri 65897, United States

Supporting Information

ABSTRACT: Intramolecular halogen bonds between aryl halide donors and suitable acceptors, such as carbonyl or quinolinyl groups, held in proximity by 1,2-aryldiyne linkers, provide triangular structures in the solid state. Aryldiyne linkers provide a nearly ideal template for intramolecular halogen bonding as minor deviations from alkyne linearity can accommodate a variety of halogen bonding interactions, including O···Cl, O···Br, O···I, N···Br, and N···I. Halogen bond lengths for these units, observed by single crystal X-ray crystallography, range from 2.75 to 2.97 Å. Internal bond angles of the semirigid bridge between halogen bond donor and acceptor are responsive to changes in the identity of the halogen, the identity of the acceptor, and the electronic environment around the halogen, with the triangles retaining almost perfect co-planarity in even the most strained systems. Consistency between experimental results and structures predicted by M06-2X/6-31G* calculations demonstrates the efficacy of this computational method for modeling halogen-bonded structures of this type.

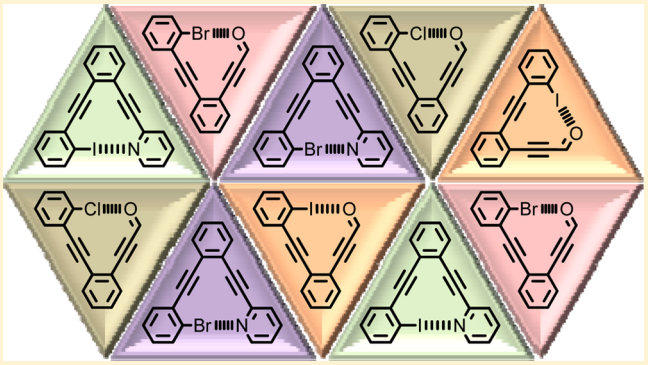

INTRODUCTION

Halogen bonding is a well-studied intermolecular force that involves the attraction of a Lewis base to an electropositive region on a halogen.[1−7] The strength of these attractions scale with the polarizability of the electron-accepting halogen, with strongest attractions to iodine and weak or no attractions to fluorine. Halogen bonding can be an important contributor in biological processes[8−11] and materials design.[12,13] The placement and identity of halogens on molecules interacting with proteins, for example, can be extremely important to drug design.[14−16] Likewise, careful incorporation of halogens onto small molecules offers opportunities for controlled crystal design[17] and supramolecular construction.[18−20] Additionally, with the development of Lewis acid catalysts,[21,22] anion sensors,[23,24] and anion transport systems,[25] researchers have started exploring the utility of this intermolecular force in solution.[26−28]

The absence of *intramolecular* halogen bonds reported in the literature speaks to the difficulties in designing such systems. The strongest halogen bond attractions occur when the electron donor is oriented directly opposite the carbon−halogen bond (i.e., O(N)···X−C angle =180°). The entropic cost of getting a remote oxygen or nitrogen lone pair to align perfectly with a halogen in a flexible molecule would be too high to account for the modest energetic gain of the halogen bond. With this in mind, we envisioned connecting these remote groups with a rigid linker to negate some of the entropic cost of intramolecular halogen bonding.

An initial concern in the design of intramolecular halogen bonding systems was the size of the non-alkyne side of the triangle. System **1** (Figure 1), for instance, is nearly perfectly triangular, as the non-alkyne side of the triangle has dimensions nearly identical to the other two sides.[29] When comparing this to reported bimolecular halogen bonding systems **2**[30] and **3**,[31] one challenge becomes obvious, namely, the size demands for the third side of the triangle are significantly larger than one would expect to be accommodated by a rigid linker.

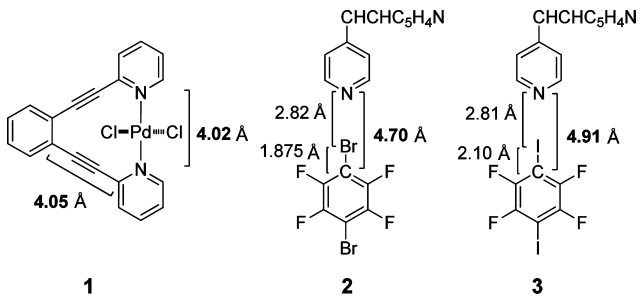

Figure 1. Comparison of spatial demands in noncovalent bridge of **1** with known bimolecular halogen bonding systems **2** and **3**.

Received: May 9, 2014
Published: June 16, 2014

 © 2014 American Chemical Society dx.doi.org/10.1021/jo501015x | J. Org. Chem. 2014, 79, 6269−6278

A second consideration in designing molecules with intramolecular halogen bonds is incorporating groups that yield the most stable "ring" structure. At first glance, the fact that the largest halogen, iodine, is expected to provide the strongest halogen bonds seems to present additional challenges. Comparisons between **2** and **3** offer some relief in this pursuit (Figure 1). Because halogen bonds become stronger as the van der Waals radius for the halogen becomes larger, these factors (bond strength vs van der Waals radius) cancel each other out so that, with all other factors being equal, similar halogen bonds are roughly the same length regardless of the halogen involved.[32] This can be seen when comparing the N···Br distance of **2** (2.82 Å) to the N···I distance of **3** (2.81 Å) (Figure 1). Consequently, only the length of the C−X bond becomes important to the spatial demands of each halogen.

Another factor that must be considered in the design of intramolecular halogen-bond-capable molecules is the electronic environment around the halogen bond donor (i.e., electron acceptor)[33] and the halogen bond acceptor (i.e., electron donor). In comparisons of bimolecular systems **3** and **4**,[31] for instance, one can see that the presence of electron-withdrawing groups near the halogen (**3**) significantly strengthens/shortens the halogen bond (Figure 2). Similarly,

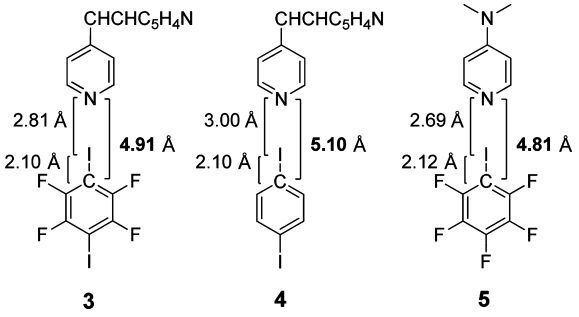

Figure 2. Cumulative effects of electron-donating and -withdrawing groups on the strength of halogen bonds.

introduction of an electron-donating group on the halogen bond acceptor side (**5**) increases the strength of this interaction.[34] Though halogen bonds are sometimes weak compared with their hydrogen bond counterparts, the attractions can be substantial when there is appropriate donor/acceptor pairing. For example, estimated interaction energies for C_6F_5X-pyridine (X = I, Br, and Cl) pairs are −5.59, −4.06, and −2.78 kcal/mol, respectively.[32]

RESULTS AND DISCUSSION

Synthesis and Design. In this study, halogen bond donors were designed with perfluorinated rings (**A**, **C**) or trifluoromethyl substituents (**B**, **D**) to maximize the electron-accepting ability of the halogen (Figure 3). Pyridinyl and carbonyl groups were initially targeted as halogen bond acceptor groups. Because the pyridinyl (**X**) systems yielded crystals that were difficult to interpret by single crystal X-ray crystallography, quinoline (**Z**) groups were installed to break up the pseudosymmetry of the triangular compounds. A benzylic ketone (**Y**) was chosen as the carbonyl moiety so that the electronics of this system might be easily manipulated in future studies by replacing the *p*-methoxy group.

All of the carbonyl systems were synthesized by a general procedure involving Sonogashira coupling of **6**, **7**, and **8**,

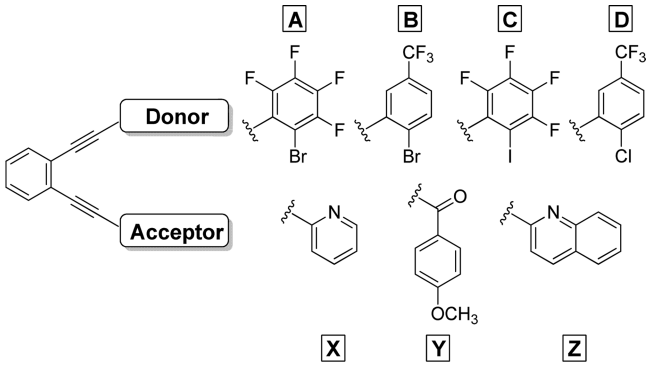

Figure 3. Different combinations of halogen bond donors and acceptors allow for a systematic study of intramolecular halogen bonding.

respectively, deprotection of the TMS-protected intermediate alkyne, and PCC oxidation of the resulting propargylic alcohol as the final step (Scheme 1).

Scheme 1. General Synthetic Sequence for Carbonyl-Based Systems

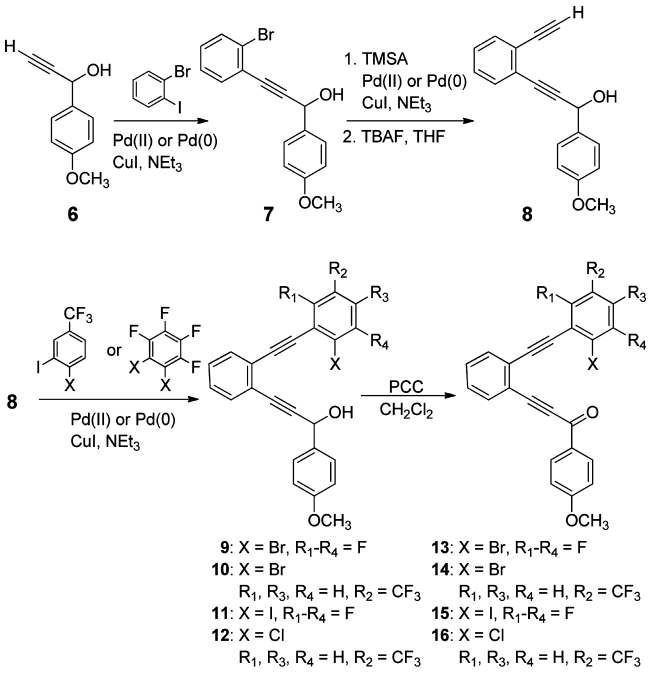

A similar reaction sequence was used to generate the quinoline derivatives from **17**[35] (Scheme 2). Syntheses of all carbonyl and quinoline compounds are relatively straightforward provided that one use a large excess of 1,2-dibromotetrafluorobenzene or 1,2-diiodotetrafluorobenzene, when needed. Sonogashira coupling with a stoichiometric amount of these reagents leads to inseparable mixtures of mono- and dicoupled products.

Proof of Concept with C═O···Br Halogen Bonding. At the outset of this project, we felt that bromoarenes offered the greatest possibility of success as the bromine atom would not be too spatially demanding but would provide relatively strong halogen bonding. To our delight, separate experiments involving single crystals of **14** (Figure 4) and **13** (Figure 5) yielded co-planar, triangular structures.

dx.doi.org/10.1021/jo501015x | J. Org. Chem. 2014, 79, 6269−6278

Scheme 2. General Synthetic Sequence for Quinoline-Based Systems

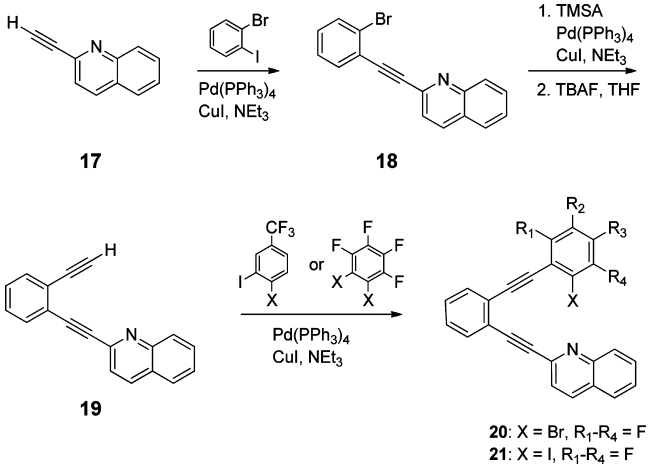

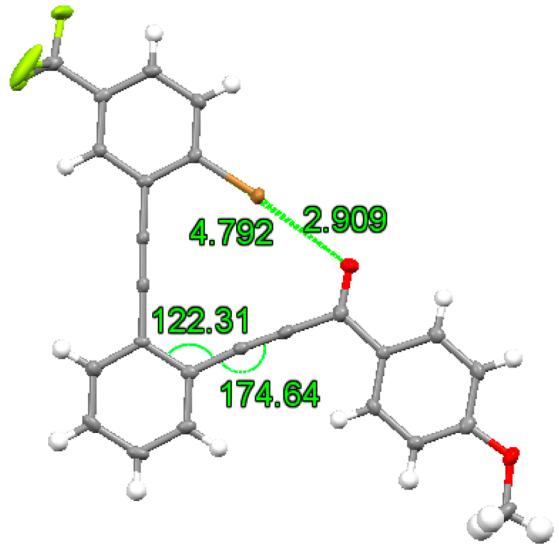

Figure 4. X-ray crystal data from **14** reveals a co-planar structure with minor deviations from ideal bond angles that accommodate intramolecular halogen bonding.

Interestingly, despite the fact that the 4.79 Å span of the C−Br···O unit in **14** and the 4.60 Å span of the C−Br···O unit in **13** are significantly larger than the ideal 4.0 Å distance, the compounds are able to form halogen bonds while retaining almost total co-planarity. The most striking difference between these two structures is the significantly shorter halogen bond interaction of 2.75 Å in **13** versus the 2.91 Å observed in **14**. This is likely a reflection of the enhanced electrostatic attraction between bromine and oxygen due to the superior electron-withdrawing capacity of the perfluorinated ring of **13** compared to the trifluoromethyl group of **14**.[32,36]

As a result of the third side of the triangle in **13** being considerably shortened, angle strain is alleviated within the ring. The largest bond angle distortions for **14** involve one of the alkyne arms bending out of linearity to 174.6° and expansion of one of the internal sp^2 bond angles to 122.3°. With the contraction of the C−Br···O span in **13**, these same bond angles relax to 177.7° and 121.7°, respectively. That these relatively modest bond angle distortions can accommodate such a significant increase in size on the third side of the

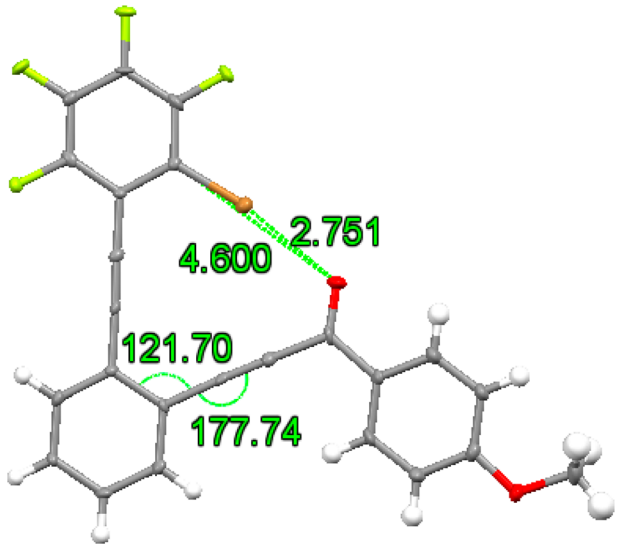

Figure 5. Crystal structure reveals that the perfluorinated ring of **13** significantly enhances the strength of the Br···O attraction compared to a similar trifluoromethyl system.

triangle (from the ideal 4.0 Å) speaks to the versatility of the 1,2-aryldiyne linker as a template for intramolecular halogen bonding.

Two other geometric parameters of interest are the C═O···Br angle around the oxygen and the C−Br···O bond angle around the halogen. Our design strategy was to place the electron-accepting halogen 120° from the carbonyl, presumably aligned with an available lone pair. Computational models predict that the ideal C═O···Br angle gradually increases as the halogen becomes more and more electropositive, with electrostatic attraction of the halogen to the highest region of electron density on the oxygen (~127°)[10,33,36] becoming the dominant interaction. While our results seem to be consistent with these predictions, with **14** displaying a C═O···Br angle of 115.7° and **13** yielding a 121.4° angle, these angles do not necessarily represent energetic minima for the halogen bonding interaction as there are other geometric constraints within the cyclic system.

It is well established in studies of halogen bonding that the ideal C−X···O(N) angle is 180°. This value stems from the location of the electropositive region of the halogen (i.e., the sigma hole) directly opposite the C−X bond. The observed C−Br···O angles for **14** and **13** are 174.5° and 171.0°, respectively. With the other variables that contribute to the overall geometry of these molecules, it is difficult to draw meaningful conclusions from these two data points. One possibility, though, is the increase in sigma hole size that goes along with enhanced electron-withdrawing effects on the halogen. Computational models predict the growth of this electropositive region as more electron-withdrawing groups act upon it. A larger sigma hole could presumably better accommodate non-ideal halogen bond angles, allowing the perfluorinated system to more significantly deviate from 180°, alleviating angle strain in the aryldiyne backbone.

Expanding Possibilities for Intramolecular Halogen Bonding. With our initial success in acquiring the two bromoarenes (**13** and **14**) described above, we set out to explore the limitations of our intramolecular halogen bonding template. The first question to be answered was whether iodo- and chloroarenes would yield similar triangular structures, or

dx.doi.org/10.1021/jo501015x | J. Org. Chem. 2014, 79, 6269−6278

Table 1. Structures Analyzed by X-ray Crystallography

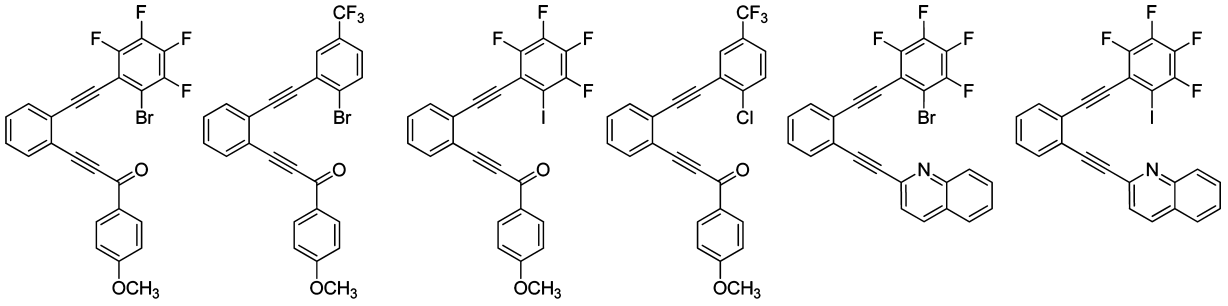

13 14 15 16 20 21

Table 2. Crystal Data for 13−16, 20, and 21[a]

	13	14	15	16	20	21
formula	$C_{24}H_{11}BrF_4O_2$	$C_{25}H_{14}BrF_3O_2$	$C_{24}H_{11}F_4IO_2$	$C_{25}H_{14}ClF_3O_2$	$C_{25}H_{10}BrF_4N$	$C_{25}H_{10}F_4IN$
FW (g mol^{-1})	487.24	483.27	534.23	438.81	480.25	527.24
crystal system	monoclinic	monoclinic	monoclinic	triclinic	monoclinic	triclinic
space group	*P*21/*c*	*P*21/*c*	*P*21/*c*	*P*-1	*P*21/*c*	*P*-1
cell lengths (Å)	*a* 5.2823(5)	*a* 9.8898(7)	*a* 10.5810(15)	*a* 7.4366(4)	*a* 11.1682(11)	*a* 8.1996(3)
	b 43.495(4)	*b* 26.9161(19)	*b* 25.437(4)	*b* 10.2527(5)	*b* 7.7306(8)	*b* 11.0966(5)
	c 9.5276(6)	*c* 7.5176(5)	*c* 7.4819(11)	*c* 13.9827(7)	*c* 21.808(2)	*c* 21.8061(9)
cell angles (deg)	*α* 90	*α* 90	*α* 90	*α* 102.2720(10)	*α* 90	*α* 76.6170(10)
	β 119.975 (4)	*β* 97.2660(10)	*β* 101.720(2)	*β* 101.0770(10)	*β* 101.726(2)	*β* 80.3790(10)
	γ 90	*γ* 90	*γ* 90	*γ* 102.5290(10)	*γ* 90	*γ* 88.7780(10)
cell volume (Å^3)	1896.21	1985.1(2)	1971.8(5)	984.72(9)	1843.5(3)	1902.75(14)
temperature (K)	99(2)	100(2)	99(2)	99(2)	99(2)	99(2)
final *R* indices [$I > 2\sigma(I)$]	R1 0.0894	R1 0.0476	R1 0.0312	R1 0.0327	R1 0.0258	R1 0.0194
	wR2 0.1790	wR2 0.1044	wR2 0.0649	wR2 0.0788	wR2 0.0654	wR2 0.0443
final *R* indices (all data)	R1 0.1088	R1 0.0656	R1 0.0421	R1 0.0420	R1 0.0316	R1 0.0217
	wR2 0.1853	wR2 0.1110	wR2 0.0689	wR2 0.0835	wR2 0.0678	wR2 0.0455
GOF	1.272	1.076	1.066	1.035	1.027	1.074

[a]All crystalline compounds were colorless. Z:4 for all samples.

Table 3. Measurements[a] from Crystal Structures of 13−16, 20, and 21

compd	X···O(N) distance (Å)	% summed van der Waals radii	C−X···O(N) distance (Å)	C−X···O(N) angle (deg)	C═O(N)···X angle (deg)	most strained C−C≡C angle (deg)	most strained aryldiyne angle (deg)
13	2.751(8)	82	4.60(1)	171.0(3)	121.4(5)	177.7(8)	121.7(7)
14	2.909(2)	86	4.792(4)	174.5(1)	115.7(2)	174.6(3)	122.3(3)
15	2.882(2)	82	4.934(4)	165.17(9)	120.5(2)	175.8(3)	121.6(3)
16	2.966(1)	91	4.694(2)	175.62(6)	114.84(9)	175.9(2)	121.7(1)
20	2.886(2)	85	4.749(2)	171.87(6)	117.6(1)	174.6(2)	122.6(2)
21[b]	2.856(2)	81	4.925(2)	168.96(6)	119.3(1)	174.7(2)	122.3(2)
	2.908(2)	82	4.983(3)	169.72(6)	117.1(1)	173.9(2)	122.8(2)

[a]Measurement uncertainties are listed in parentheses. [b]There are two unique molecules of **21** in the asymmetric unit; measurements are shown for both.

was bromine, in fact, the perfect compromise of size and halogen bonding ability. Single crystals of **15** and **16** provided evidence that the 1,2-aryldiyne bridge is flexible enough to accommodate chloro-, bromo-, and iodo-substituents, while maintaining near perfect co-planarity.

The second question to be answered was whether the halogen bond acceptor (i.e., electron donor) is interchangeable. Initial studies with pyridine were promising but provided crystals that were difficult to interpret via X-ray crystallography. Fortunately, elaboration of our simple pyridine strategy to quinoline-based systems provided two samples (**20** and **21**) that were suitable for X-ray characterization (see Tables 1 and 2).

Having generated a number of systems capable of intramolecular halogen bonding, the third question that arose was whether the template being used was flexible enough to allow for "natural" halogen bonding, or were the bond lengths and angles observed overly constrained by the rigid linker. In order to answer this question, we investigated the trends observed for the new systems and compared those to observations and predictions from prior studies of *intermolecular* halogen bonding and our own computational predications.

Trends Observed for Intramolecular Halogen Bonding. *Halogen Bond Strength.* As discussed above, larger halogen atoms are expected to form stronger halogen bonds. This trend cannot necessarily be correlated to bond lengths. A large halogen with a strong attraction to an acceptor might

dx.doi.org/10.1021/jo501015x | J. Org. Chem. 2014, 79, 6269−6278

Table 4. Computed[a] Structures of 13−16, 20, and 21

compd	X···O(N) distance (Å)	% summed van der Waals radii	C−X···O(N) distance (Å)	C−X···O(N) angle (deg)	C═O(N)···X angle (deg)	most strained C−C≡C angle (deg)
13	2.86	85	4.72	172.1	116.9	177.0
14	2.89	86	4.76	173.1	115.9	176.7
15	2.90	83	4.96	166.3	118.9	176.3
16	2.89	88	4.61	173.6	118.2	177.7
20	2.89	85	4.75	172.2	117.3	175.4
21	2.96	84	5.03	168.6	115.4	174.4

[a]Calculated using M06-2X functional and 6-31G* basis set. Small (28-electron) core Dirac−Fock (MDF) effective-core pseudo potential and corresponding basis set used for iodine.

display a halogen bond length similar to that of a smaller halogen with a weaker attraction to that acceptor. This is evident in the first data column of Table 3, with all systems except **13** displaying a halogen bond distance of roughly 2.9 Å.

A better indicator of halogen bond strength is how the length of the halogen bond compares to the sum of the van der Waals radii of the atoms involved. The second data column of Table 3 quantifies this as the percent of the summed van der Waals radii (N = 1.55 Å, O = 1.52 Å, Cl = 1.75 Å, Br = 1.85 Å, I = 1.98 Å).[37] Not surprisingly, the strongest halogen bonds (other than **13**) come from iodo-systems **15** and **21**, and the weakest come from chloro-system **16**. Interestingly, the perfluorinated-bromo-quinoline system **20** is more comparable to the trifluoromethyl-bromo-carbonyl system **14** than the other perfluorinated-bromo compound **13**. This observation is inconsistent with that fact that the more basic quinoline is expected to be a better acceptor than a carbonyl. One possible reason for elongation of halogen bonds in quinoline systems **20** and **21** is steric interactions between the neighboring fluorine atom of the haloarene and a nearby hydrogen from the quinoline ring. Similar secondary interactions of perfluorinated rings have been invoked in explanations of anomalous *intermolecular* halogen bond measurements.[33]

Halogen Bond Angle (C−X···O(N)). The dimensions of each triangle likely result from a balance between minimizing angle strain and maximizing halogen bond attractions. One mechanism for angle strain relief may be deviation of the C−X···O(N) angle from the optimal 180°. The degree to which each halogen accommodates non-ideal angles is based upon the size of the sigma hole. The largest sigma holes are expected to be found on the largest halogen atoms and on those halogens that have the strongest electron-withdrawing groups acting upon them. Careful inspection of the fourth data column of Table 3 reveals a clear trend that supports this expectation. Specifically, in terms of halogen bonds that have the largest deviations from linearity, the compounds rank iodo-systems > perfluorinated-bromo-systems > trifluoromethyl-bromo-system > chloro-system. The fact that this trend opposes predictions that suggest the magnitude of the directionality of a halogen bond correlates with the magnitude of the attraction[32] may indicate that this parameter (i.e., C−X···O(N) bond angle) is dominated by relief of angle strain in our synthetic systems.

A consequence of these deviations from linearity may be artificially elongated halogen bonds in the iodo-systems. For example, one peculiarity in the halogen bond strengths noted in Table 3 is the apparent equivalence in halogen bond strengths between **13**, a bromoarene, and **15**, an iodoarene. It is well established that the strongest halogen bonds form when the acceptor is oriented 180° from the C−X bond. Halogen bonds become weaker the more they deviate from this arrangement. The two iodoarenes systems in this study, **15** and **21**, stray the most from this ideal bond angle. Consequently, the strengths of these iodoarene halogen bonds are likely weaker, and therefore longer, than optimal.

Angle around the Carbonyl (C═O···X). Another location where deviations from ideal angles may serve to balance the negative effects of angle strain with the positive effects of the halogen bond attraction is the carbonyl oxygen. While it is difficult to fully understand how much of this measurement is dictated by alleviation of angle strain, there is an interesting correlation between the angles recorded in data column 5 of Table 3 and predicted trends. Halogen bonding is thought to be a result of a mixture of electrostatic attraction and dispersion.[38,39] The optimal geometry of a halogen bond can depend on the relative contribution of each of these attractive forces. Computational results suggest that as the electrostatic contribution increases so does the bond angle around the carbonyl, until the highest area of electron density is reached around 127°.[36] Analysis of the first four rows of data column five in Table 3 reveals angles that are consistent with this trend. Specifically, the molecules that contain the best electron acceptors, **13** and **15**, display the largest C═O···X bond angles (∼121°). The worst electron acceptors in **14** and **16** yield much smaller C═O···X angles (∼115°).

Flexible Nature of the 1,2-Aryldiyne Bridge. One of the earliest concerns in the design of this project was the feasibility of squeezing a C−X···O(N) unit, that we predicted to span roughly 5 Å, into a "rigid" system that should only accommodate 4 Å. Literature and past experience suggest that alkyne linkers are surprisingly flexible. The current study reflects this, with alkynyl geometries up to 6° away from linear (data column 6, Table 4). Interestingly, the cumulative effect of these fairly modest deviations is the ability to accommodate a wide range of spatial demands. The triangular structures maintain nearly perfect co-planarity in systems ranging from 4.6 to 5.0 Å (data column 3, Table 4) on the third side of the triangle. This combination of flexibility and rigidity allows the aryldiyne bridge to template a wide variety of intramolecular halogen bonding interactions while minimizing the entropic cost of bringing donors and acceptors into proximity.

Computed Predictions versus Experimental Results. Computational models of the target compounds were studied for two reasons. First, we wanted to find a method and basis set that were suitable for study of these relatively large halogen bonding systems. Comparing our calculated and experimental results would allow an assessment of the chosen computational method. Second, accompanying calculations might allow us to take a closer look at each experimental data point to identify solid-state structural features that may not be consistent with gas-phase minima.

dx.doi.org/10.1021/jo501015x | J. Org. Chem. 2014, 79, 6269−6278

The M06-2X functional with a 6-31G* basis set (for atoms other than iodine) seems to be sufficient for modeling these systems. Half of the predicted halogen bond lengths (**14**, **15**, and **20**), for instance, are within 0.02 Å of their corresponding experimental values. The largest deviations from experiment are with **13** and **16**, where the calculations overestimate and underestimate, respectively, halogen bond lengths by approximately 0.1 Å. In other words, the calculations underestimate the strength of the halogen bond in the perfluoro-bromo-carbonyl system, **13**, and overestimate the strength of the halogen bond in the trifluoromethyl-chloro-carbonyl system, **16**.

Disagreements between computed and experimental results are not necessarily an indictment of the computational method. Measurements from crystal structures may relate to the lowest energy conformations of the individual molecules, but the effects of crystal packing cannot be ignored. This is most apparent in a careful analysis of the torsions between the alkyne-linked units of each molecule. Computationally, the conjugated portions of the targeted structures are predicted to be perfectly planar, with the largest calculated torsion at 0.5°. Although all structures are nearly planar in the solid state, torsions around the alkyne-linked units range from 0 to 7°, which may partly explain the computational overestimation of some halogen bond strengths.

Slight deviations from planarity are likely due to crystal packing effects. Packing in the trifluoro-bromo-carbonyl (**14**) crystal provides an illustration of this (Figure 6). One stacking

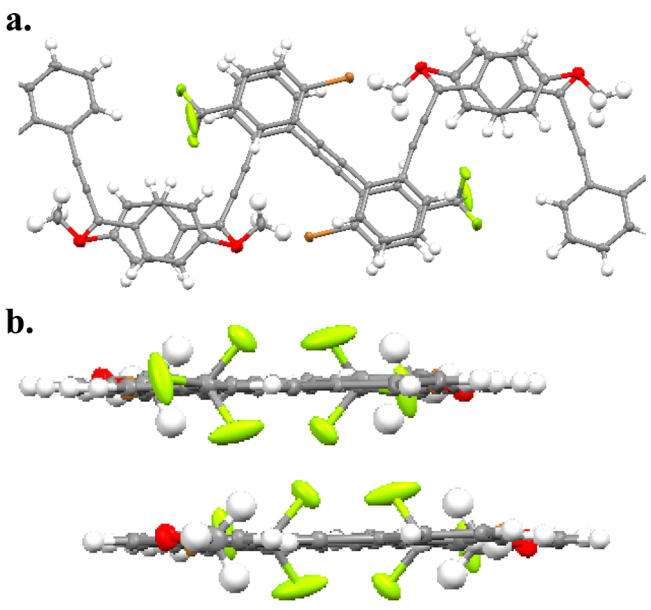

Figure 6. (a) View of packing of **14** along the *c*-axis shows the antiparallel stacking of 4-methoxybenzoyl groups in neighboring layers. (b) View of packing of **14** along the *b*-axis shows the qualitative co-planarity of each layer with the exception of tetrahedral methoxy and trifluoromethyl substituents.

feature that is common to most of the carbonyl systems studied is the canceling of strong dipoles in the 4-methoxybenzoyl groups. When these groups stack on top of each other, the methoxy group of one molecule is placed in the proximity of the carbonyl of a molecule in the neighboring layer (Figure 6a). Through-space interactions of the methoxy hydrogens of one layer with ketone groups of the next layer (distance = 2.71 Å) likely diminish the co-planarity of the carbonyl regions, skewing the observed geometries away from ideal.

CONCLUSIONS

A template for *intramolecular* halogen bonding has been developed from 1,2-aryldiynes. The conjugated bridging unit is rigid enough to negate some of the entropic cost that would normally be associated with this type of remote intramolecular attraction. At the same time, the aryldiyne unit is flexible enough to accommodate a number of different halogen bonding motifs, while maintaining near perfect planarity. The versatility of the template provides an opportunity for dissecting some of the most important parameters for this attractive force.

Calculations using the M06-2X functional with a 6-31G* basis set (for atoms other than iodine) provide satisfactory halogen bonding predictions for these relatively large systems. The most significant disagreements between the gas-phase calculations and the experimental, solid-state structures likely arise from packing anomalies in the crystalline samples.

EXPERIMENTAL SECTION

Crystallization. Compounds **13**, **15**, **16**, and **20** were recrystallized from absolute ethanol. In each case, approximately 4 mg of the target compound was placed in a screw-cap vial and dissolved, with heating, in 4 mL of boiling ethanol. The vial was sealed and allowed to cool to room temperature and left undisturbed for several days. At this stage the crystals were removed and analyzed. Compound **14** was recrystallized in the same way from hexane solution. Compound **21** was recrystallized from acetonitrile by first dissolving 5 mg in 100 mL of refluxing acetonitrile and allowing the resultant solution to stand undisturbed for several days at which stage crystals suitable for X-ray analysis had formed.

X-ray Structure Determination. For each compound a single crystal was mounted on a Kryoloop using viscous hydrocarbon oil. Data was collected using a CCD diffractometer equipped with Mo Kα radiation with λ = 0.71073 Å. Data collection at low temperature was facilitated by use of a Kryoflex system with an accuracy of ±1 K. Initial data processing was carried out using the Apex II software suite.[40] Structures were solved by direct methods using SHELXS-2013 and refined against F2 using SHELXL-2013.[41] In all structures, hydrogen atoms were located in the difference maps but were placed in idealized positions and refined with a riding model. The program X-Seed was used as a graphical interface during refinement.[42]

Computational Methods. Gas-phase geometry optimizations of the halogen-bonded molecules were performed with the Gaussian 09 suite of programs[43] using M06-2X.[44] The M06-2X functional was chosen as it has been shown to give good results for halogen-bonded systems.[45] The 6-31G* basis set[46] was used for all atoms except iodine, for which the small (28-electron) core Dirac–Fock (MDF) effective-core pseudo potential and the corresponding basis sets were used.[47] All structures were verified to be local minima through vibrational frequency analysis.

General Reaction Considerations. All starting materials and reagents were either commercially available or readily synthesized following literature procedures. Dry, air-free triethylamine was acquired via distillation from CaH_2 under a nitrogen atmosphere. Dry, air-free THF was acquired by placing THF from a solvent purification system (under N_2) into a sealed flask containing activated 3 Å sieves. This flask was stored under a positive pressure of N_2. All Sonogashira reactions were performed using sealed, side-arm storage tubes under an argon atmosphere. TMS-deprotection reactions were performed with TBAF at −89 °C (liq N_2/2-propanol), as these conditions typically give higher yields, in a shorter period of time, than standard K_2CO_3/MeOH deprotection reactions. The targeted compounds have limited solubility in most solvents but are most soluble in halohydrocarbon solvents (CH_2Cl_2 or $CHCl_3$/$CDCl_3$).

dx.doi.org/10.1021/jo501015x | J. Org. Chem. 2014, 79, 6269–6278

Even with these optimal solvents, creating concentrations that allowed complete ^{13}C NMR characterization was difficult (e.g., **20**). In these cases, ^{1}H NMR, APCI-QTOF, and X-ray data were sufficient to confirm the identity of the compounds.

Synthetic Procedures. *1-(4-Methoxyphenyl)prop-2-yn-1-ol (**6**).* In accord with published procedure,[48] 7.48 mL (18.7 mmol) *n*-BuLi solution (2.5 M in hexane) was added dropwise to a chilled (−89 °C, liq N_2/2-propanol) solution of (trimethylsilyl)acetylene (2.83 mL, 20.0 mmol) in 30 mL THF under an atmosphere of argon. After 40 min at this temperature, 2.0 mL (16.4 mmol) *p*-anisaldehyde was added dropwise via syringe. After the mixture warmed to room temperature for 4 h, water was added to quench the reaction. The aqueous layer was extracted twice with ethyl acetate. The combined organic layers were dried with anhydrous Na_2SO_4, filtered, and concentrated. Methanol (30 mL) and K_2CO_3 (until saturation) were added to this crude residue. After stirring 18 h at room temperature, methanol was removed under reduced pressure. The crude residue was purified by flash chromatography (silica, 70% hexane/30% EtOAc) to yield 2.25 g (13.9 mmol, 84.2% yield) colorless oil. ^{1}H NMR (400 MHz, $CDCl_3$): δ 7.45 (d, J = 8.7 Hz, 2H), 6.89 (d, J = 8.7 Hz, 2H), 5.39 (s, 1H), 3.79 (s, 3H), 2.65 (d, J = 2.2 Hz, 1H), 2.51 (br s, 1H) ppm. ^{13}C NMR (100 MHz, $CDCl_3$) δ 159.7, 132.4, 128.1, 114.0, 83.7, 74.6, 64.0, 55.3 ppm. APCI-QTOF (m/z) calcd for $C_{10}H_{10}O_2H^+$ 163.0754; found 163.0747.

*3-(2-Bromophenyl)-1-(4-methoxyphenyl)prop-2-yn-1-ol (**7**).* Terminal alkyne **6** (2.25 g, 13.9 mmol) was dissolved in 20 mL dry THF and transferred to an air-free storage tube under Ar. Freshly distilled triethylamine (10 mL) and 2-bromoiodobenzene (1.78 mL, 13.9 mmol) were added separately via syringe. Argon was bubbled through this mixture for 15 min. CuI (0.132 g, 0.70 mmol) and $Pd(PPh_3)_4$ (0.80 g, 0.70 mmol) were added, and the tube was sealed and stirred at room temperature for 20 h. The mixture was taken up in CH_2Cl_2. This organic mixture was washed with NH_4Cl solution, dried with anhydrous Na_2SO_4, filtered, and concentrated. This crude residue was purified by flash chromatography (silica, 10% EtOAc/90% hexane) to yield 4.28 g orange oil (13.5 mmol, 97.1% yield). ^{1}H NMR (400 MHz, $CDCl_3$): δ 7.58 (m, 3H), 7.48 (dd, J = 7.7, 1.5 Hz, 1H), 7.24 (td, J = 7.7, 1.1 Hz, 1H), 7.16 (td, J = 7.7, 1.7 Hz, 1H), 6.91 (m, 2H), 5.67 (d, J = 6.4 Hz, 1H), 3.80 (s, 3H), 2.53 (d, J = 6.4 Hz, 1H) ppm. ^{13}C NMR (100 MHz, $CDCl_3$) δ 159.7, 133.6, 132.6, 132.4, 129.7, 128.4, 127.0, 125.6, 124.7, 114.0, 93.5, 85.0, 64.8, 55.3 ppm. APCI-QTOF (m/z) calcd for $C_{16}H_{12}BrO_2^-$ 315.0021/317.0000; found 315.0015/317.0040.

*3-(2-Ethynylphenyl)-1-(4-methoxyphenyl)prop-2-yn-1-ol (**8**).* Bromoarene **7** (4.28 g, 13.5 mmol) was dissolved in 10 mL dry THF and transferred to an oven-dried storage tube under Ar. Another 10 mL THF was added, followed by 10 mL freshly distilled NEt_3. Argon was bubbled through this mixture for 15 min. $Pd(PPh_3)_4$ (0.67 g, 0.58 mmol) and CuI (0.13 g, 0.68 mmol) were added, followed by 2.12 mL (15.0 mmol) TMS-acetylene. The tube was sealed and heated at 80 °C for 18 h. After cooling to room temperature, the mixture was rinsed into a separatory funnel with CH_2Cl_2. This organic mixture was washed with NH_4Cl solution, dried with anhydrous Na_2SO_4, filtered, and concentrated. The crude residue was purified via flash chromatography (silica, 15% EtOAC/85% hexane) to yield the TMS-protected intermediate as an orange-red oil (2.54 g, 7.59 mmol, 56.2% yield). ^{1}H NMR (400 MHz, $CDCl_3$): δ 7.58 (d, J = 8.7 Hz, 2H), 7.47 (m, 2H), 7.26 (m, 2H), 6.91 (d, J = 8.7 Hz, 2H), 5.68 (d, J = 6.2 Hz, 1H), 3.81 (s, 3H), 2.28 (d, J = 6.2 Hz, 1H) ppm. ^{13}C NMR (100 MHz, $CDCl_3$) δ 159.8, 132.9, 132.4, 132.0, 128.4, 128.22, 128.21, 125.7, 125.3, 114.1, 103.4, 98.7, 92.9, 85.2, 64.9, 55.4, 0.05 ppm. APCI-QTOF (m/z) calcd for $C_{21}H_{22}O_2SiH^+$ 335.1462; found 335.1468. The TMS-protected intermediate (2.54 g, 7.59 mmol) was dissolved in 40 mL THF. After cooling the mixture to −89 °C (2-propanol/liq N_2), 7.60 mL of a 1 M TBAF solution (in THF) was added dropwise via syringe. After 1 h, NH_4Cl solution was added to the cold mixture. After warming to room temperature, the mixture was rinsed into a separatory funnel with CH_2Cl_2. After separation of the layers, the aqueous layer was again extracted with CH_2Cl_2. The combined organic layers were dried with anhydrous Na_2SO_4, filtered, and concentrated. This crude residue was loaded onto a flash column (silica, 50% EtOAc/50% hexane) with a minimal amount of CH_2Cl_2. The product was isolated as an orange-red oil (1.99 g, 0.759 mmol, 100% yield). ^{1}H NMR (400 MHz, $CDCl_3$): δ 7.60 (d, J = 8.7 Hz, 2H), 7.50 (m, 2H), 7.29 (m, 2H), 6.91 (d, J = 8.7 Hz, 2H), 5.68 (d, J = 5.4 Hz, 1H), 3.81 (s, 3H), 3.29 (s, 1H), 2.41 (d, J = 6.0 Hz, 1H) ppm. ^{13}C NMR (100 MHz, $CDCl_3$) δ 159.7, 132.8, 132.6, 132.1, 128.5, 128.4, 128.3, 125.5, 124.8, 113.9, 93.0, 84.9, 82.2, 81.2, 64.8, 55.3 ppm. APCI-QTOF (m/z) calcd for $C_{18}H_{13}O_2^-$ 261.0921; found 261.0912.

*2-((2-Bromophenyl)ethynyl)quinoline (**18**).* Terminal alkyne **17**[35] (0.600 g, 3.92 mmol) was added to a storage tube under argon. $Pd(PPh_3)_4$ (0.23 g, 0.20 mmol) and CuI (0.037 g, 0.20 mmol) were added, followed by 20 mL dry, deoxygenated THF and 5 mL freshly distilled NEt_3. After 1-bromo-2-iodobenzene (0.503 mL, 3.92 mmol) was added, and the tube was sealed and heated at 50 °C for 1 day. Upon cooling to room temperature, the mixture was rinsed into a separatory funnel with CH_2Cl_2. The organic phase was washed with NH_4Cl solution, dried with anhydrous Na_2SO_4, filtered, and concentrated. The product was purified by flash chromatography (silica, 1% EtOAc/99% toluene) to reveal an orange oil (0.641 g, 2.08 mmol, 53% yield). ^{1}H NMR (400 MHz, $CDCl_3$): δ 8.12 (d, J = 8.5 Hz, 1H), 8.06 (d, J = 8.4 Hz, 1H), 7.69 (m, 3H), 7.60 (m, 2H), 7.49 (m, 1H), 7.27 (td, J = 7.6, 1.2 Hz, 1H), 7.17 (td, J = 7.7, 1.7 Hz, 1H) ppm. ^{13}C NMR (100 MHz, $CDCl_3$) δ 148.1, 143.2, 136.1, 133.8, 132.4, 130.2, 130.0, 129.3, 127.5, 127.2, 127.13, 127.08, 126.0, 124.5, 124.3, 93.5, 88.2 ppm. APCI-QTOF (m/z) calcd for $C_{17}H_{10}BrNH^+$ 308.0075/310.0054; found 308.0073/310.0053.

*2-((2-Ethynylphenyl)ethynyl)quinoline (**19**).* Bromoarene **18** (0.641 g, 2.08 mmol) was dissolved in 20 mL dry THF and transferred to a storage tube under Ar. Freshly distilled NEt_3 (5 mL) was added, and argon was bubbled through the mixture for 20 min. Sequentially, $Pd(PPh_3)_4$ (0.116 g, 0.10 mmol), CuI (0.019 g, 0.10 mmol), and TMS-acetylene (0.424 mL, 3.0 mmol) were added. The tube was sealed and heated at 90 °C for 24 h. Upon cooling to room temperature, the mixture was rinsed into a separatory funnel with CH_2Cl_2. The organic phase was washed with NH_4Cl solution, dried with anhydrous Na_2SO_4, filtered, and concentrated. The crude mixture was purified via flash chromatography (silica, 1% EtOAc/99% toluene) to reveal the TMS-protected intermediate as a dark red oil (0.473 g, 1.45 mmol, 70% yield). ^{1}H NMR (400 MHz, $CDCl_3$): δ 8.13 (d, J = 8.4, 1H), 8.12 (d, J = 8.3, 1H), 7.78 (d, J = 8.1 Hz, 1H), 7.72 (m, 1H), 7.65 (m, 2H), 7.53 (m, 2H), 7.31 (m, 2H), 0.29 (s, 9H) ppm. ^{13}C NMR (100 MHz, $CDCl_3$) δ 148.2, 143.6, 135.9, 132.29, 132.26, 130.0, 129.4, 128.7, 128.2, 127.5, 127.1, 126.3, 124.9, 124.5, 103.2, 99.1, 93.0, 88.6, 0.0 ppm. APCI-QTOF (m/z) calcd for $C_{22}H_{19}NSiH^+$ 326.1360; found 326.1360. The TMS-protected alkyne (0.473 g, 1.45 mmol) was dissolved in 30 mL THF and cooled to −89 °C (2-propanol/liq N_2). TBAF (1.45 mL 1 M solution in THF) was added dropwise, and the mixture was stirred for 1 h. The mixture was rinsed into a separatory funnel with ethyl acetate. This organic mixture was washed with H_2O, dried with an anhydrous Na_2SO_4, filtered, and concentrated. The resulting residue was purified via flash chromatography (10% EtOAc/90% toluene) to reveal **19** as a brown solid (0.358 g, 1.41 mmol, 97% yield). ^{1}H NMR (400 MHz, $CDCl_3$): δ 8.12 (d, J = 8.5 Hz, 1H), 8.10 (d, J = 8.5 Hz, 1H), 7.76 (d, J = 8.2 Hz, 1H), 7.70 (m, 2H), 7.62 (d, J = 8.4 Hz, 1H), 7.53 (m, 2H), 7.33 (m, 2H), 3.44 (s, 1H) ppm. ^{13}C NMR (100 MHz, $CDCl_3$) δ 148.2, 143.5, 136.0, 132.6, 132.5, 130.0, 129.4, 128.8, 128.6, 127.5, 127.2, 125.3, 125.2, 124.7, 93.1, 88.3, 82.0, 81.7 ppm. APCI-QTOF (m/z) calcd for $C_{19}H_{11}NH^+$ 254.0964; found 254.0968.

*3-(2-((2-Bromo-3,4,5,6-tetrafluorophenyl)ethynyl)phenyl)-1-(4-methoxyphenyl)prop-2-yn-1-one (**13**).* Terminal alkyne **8** (0.214 g, 0.82 mmol) was rinsed into an air-free storage tube under Ar with freshly distilled NEt_3 (20 mL). Sequentially, $Pd(PPh_3)_4$ (44 mg, 0.038 mmol), CuI (3.9 mg, 0.020 mmol), and 1,2-dibromo-3,4,5,6-tetrafluorobenzene (0.412 mL, 3.0 mmol) were added. The tube was sealed and heated at 80 °C for 4 days. After cooling to room temperature, the mixture was diluted with EtOAc and washed with water. The organic phase was separated, dried with Na_2SO_4, filtered, and concentrated. The crude residue was dissolved in a minimal

dx.doi.org/10.1021/jo501015x | J. Org. Chem. 2014, 79, 6269−6278

amount of $CHCl_3$ and loaded onto a flash column (silica, 20% EtOAc/80% hexane). Isolation of the appropriate fractions yielded alcohol intermediate **9** as a white solid (0.235 g, 0.48 mmol, 58.6% yield). ^{1}H NMR (400 MHz, $CDCl_3$): δ 7.60 (m, 1H), 7.54 (m, 3H), 7.36 (m, 2H), 6.83 (m, 2H), 5.69 (d, J = 6.2 Hz, 1H), 3.79 (s, 3H), 2.23 (d, J = 6.2 Hz, 1H) ppm. ^{13}C NMR (100 MHz, $CDCl_3$) extensive fluorine coupling makes ^{13}C signals of fluorinated ring impossible to accurately interpret at achievable concentrations, δ 159.7, 132.7, 132.4, 132.3, 129.3, 128.4, 128.3, 125.3, 124.4, 113.9, 99.6 (coupled), 93.7, 84.5, 82.3 (coupled), 64.9, 55.3 ppm. ^{19}F NMR (376.4 MHz, $CDCl_3$) δ −128.4 (ddd, J = 22.0, 9.4, 3.4 Hz), −132.0 (ddd, J = 21.1, 9.4, 3.4 Hz), −151.7 (m), −155.5 (m) ppm. APCI-QTOF (m/z) calcd for $C_{24}H_{13}BrF_4O_2H^+$ 489.0113/491.0093; found 489.0001/491.0081. Intermediate alcohol **9** (0.235 g, 0.48 mmol) was dissolved in 40 mL dry CH_2Cl_2. To this were added 3 Å molecular sieves (0.28 g), Celite (0.2 g), and PCC (0.140 g, 0.65 mmol). After the mixture was stirred at room temperature for 24 h, another portion of PCC (0.055 g, 0.26 mmol) was added, and the mixture was stirred for 3 days at room temperature. The reaction mixture was filtered through a plug of silica and the filtrate concentrated under reduced pressure. The crude residue was dissolved in a minimal amount of CH_2Cl_2 and loaded onto a flash column (silica, 25% EtOAc/75% hexane). The product was isolated as an off-white solid (0.147 g, 0.30 mmol, 63% yield). Additional purification can be achieved via prep TLC (silica, 30% EtOAc/70% hexane) when necessary. ^{1}H NMR (400 MHz, $CDCl_3$): δ 8.21 (d, J = 8.9 Hz, 2H), 7.72 (m, 2H), 7.48 (m, 2H), 6.87 (d, J = 8.9 Hz, 2H), 3.87 (s, 3H) ppm. ^{13}C NMR (100 MHz, $CDCl_3$) extensive fluorine coupling makes ^{13}C signals of fluorinated ring and neighboring alkyne impossible to accurately interpret at achievable concentrations, δ 176.4, 164.5, 133.6, 132.9, 132.2, 130.3, 130.2, 129.5, 125.30, 123.25, 113.7, 90.5, 89.7, 55.5 ppm. ^{19}F NMR (376.4 MHz, $CDCl_3$) δ −128.1, (ddd, J = 21.8, 9.5, 1.1 Hz), −131.3 (ddd, J = 20.7, 9.4, 2.8 Hz), −151.1 (m), −155.4 (m). APCI-QTOF (m/z) calcd for $C_{24}H_{11}BrF_4O_2H^+$ 486.9957/488.9936; found 486.9946/488.9930.

*3-(2-((2-Bromo-5-(trifluoromethyl)phenyl)ethynyl)phenyl)-1-(4-methoxyphenyl)prop-2-yn-1-one (**14**).* Terminal alkyne **8** (0.200 g, 0.76 mmol) was dissolved in dry THF (6 mL) and transferred to a storage tube under argon. 1-Bromo-2-iodo-4-(trifluoromethyl)benzene (0.267 g, 0.76 mmol) was dissolved in a mixture of dry THF (4 mL) and freshly distilled NEt_3 (5 mL) and transferred to the same storage tube. Argon was bubbled through this mixture for 15 min. $Pd(PPh_3)_4$ (46 mg, 0.040 mmol) and CuI (7.6 mg, 0.040 mmol) were added, and the tube was sealed and heated at 40 °C for 3 days. After cooling to room temperature, the mixture was rinsed into a separatory funnel with CH_2Cl_2. The organic mixture was washed with NH_4Cl solution, and this aqueous phase was back-extracted with CH_2Cl_2. The combined organic layers were dried with anhydrous Na_2SO_4, filtered, and concentrated. The crude residue was purified via flash chromatography (silica, 50% CH_2Cl_2, 50% hexane increased gradually to 100% CH_2Cl_2) to reveal alcohol intermediate **10** as a colorless oil (0.261 g, 0.54 mmol, 70.6% yield). ^{1}H NMR (400 MHz, $CDCl_3$): δ 7.76 (d, J = 1.8 Hz, 1H), 7.70 (d, J = 8.4 Hz, 1H), 7.59 (m, 1H), 7.53 (m, 3H), 7.38 (dd, J = 8.4, 1.9 Hz, 1H), 7.32 (m, 2H), 6.78 (d, J = 8.7 Hz, 2H), 5.70 (d, J = 6.2 Hz, 1H), 3.74 (s, 3H), 2.43 (d, J = 6.2 Hz, 1H) ppm. ^{13}C NMR (100 MHz, $CDCl_3$) δ 159.7, 133.1, 132.7, 132.31, 132.28, 130.2 (q, J = 3.7 Hz), 130.0, 129.7, 129.3, 128.8, 128.4, 128.3, 126.3, 125.8 (q, J = 3.7 Hz), 125.2, 124.9, 123.4 (q, J = 271 Hz), 94.0, 93.4, 90.3, 84.9, 64.9, 55.2 ppm. APCI-QTOF (m/z) calcd for $C_{25}H_{15}BrF_3O_2^-$ 483.0208/485.0187; found 483.0199/485.0225. Intermediate alcohol **10** (0.198 g, 0.407 mmol) and PCC (0.088 g, 0.41 mmol) were dissolved in 30 mL CH_2Cl_2. After 22 h at room temperature, the solvent was removed under reduced pressure. The remaining residue was purified via flash chromatography (silica, 100% CH_2Cl_2) to reveal the product as a white solid (0.168 g, 0.347 mmol, 85.2% yield). ^{1}H NMR (400 MHz, $CDCl_3$): δ 8.24 (d, J = 8.9 Hz, 2H), 7.79 (d, J = 1.9 Hz, 1H), 7.74 (m, 2H), 7.68 (d, J = 7.5 Hz, 1H), 7.45 (m, 3H), 6.75 (d, J = 8.9 Hz, 2H), 3.79 (s, 3H) ppm. ^{13}C NMR (100 MHz, $CDCl_3$) δ 176.5, 164.5, 133.7, 133.2, 132.6, 132.1, 130.3, 130.1, 129.8, 129.1, 126.16, 126.13, 126.0, 123.3 (q, J = 271 Hz), 123.2, 113.8, 93.4, 91.3, 90.5, 90.0, 55.4 ppm. APCI-QTOF (m/z) calcd for $C_{25}H_{14}BrF_3O_2H^+$ 483.0208/485.0187; found 483.0215/485.0197.

*1-(4-Methoxyphenyl)-3-(2-((2,3,4,5-tetrafluoro-6-iodophenyl)-ethynyl)phenyl)prop-2-yn-1-one (**15**).* Terminal alkyne **8** (0.093 g, 0.35 mmol) was rinsed into an argon-flushed storage tube with freshly distilled NEt_3 (30 mL). 1,2-Diiodotetrafluorobenzene (0.40 g, 1.00 mmol), $Pd(PPh_3)_4$ (13.2 mg, 0.011 mmol), and CuI (2.1 mg, 0.011 mmol) were added, and the tube was sealed under argon and heated at 90° for 20 h. After cooling to room temperature, the mixture was rinsed into a flask with ethyl acetate. This organic mixture was dried with anhydrous Na_2SO_4, filtered, and concentrated. The resulting residue was purified by flash chromatography (silica, 5% EtOAc/95% toluene) to reveal a white solid (0.11 g) that proved to be a mixture of desired alcohol **11** and a small amount of reduced material (C−I → C−H). This mixture was taken on to the oxidation step without further purification. The impure alcohol was dissolved in 30 mL dry CH_2Cl_2 and mixed with Celite (1.3 g) and PCC (0.054 g, 0.25 mmol). After 24 h of stirring at room temperature, the mixture was filtered through a pad of Celite. The filtrate was concentrated and purified by sequential flash chromatography (silica, 1% EtOAc/99% toluene) and prep TLC (silica, 5% EtOAc/95% toluene). The product was isolated as a white solid (0.054 g, 0.101 mmol, 29% yield over two steps). ^{1}H NMR (400 MHz, $CDCl_3$): δ 8.20 (d, J = 8.8 Hz, 2H), 7.73 (m, 2H), 7.49 (m, 2H), 6.86 (d, J = 8.8 Hz, 2H), 3.87 (s, 3H) ppm. ^{13}C NMR (100 MHz, $CDCl_3$) extensive fluorine coupling makes ^{13}C signals of fluorinated ring and neighboring alkyne impossible to accurately interpret at achievable concentrations, δ 176.5, 164.6, 133.8, 133.0, 132.2, 130.3, 130.2, 129.4, 125.4, 123.1, 113.7, 90.5, 90.2, 55.5 ppm. ^{19}F NMR (376.4 MHz, $CDCl_3$) δ −113.5 (ddd, J = 22.9, 11.5, 3.8 Hz), −129.7 (ddd, J = 20.7, 9.8, 3.8 Hz), −150.7 (m), −154.0 (td, J = 20.3, 3.8 Hz) ppm. APCI-QTOF (m/z) calcd for $C_{24}H_{11}F_4IO_2H^+$ 534.9818; found 534.9806.

*3-(2-((2-Chloro-5-(trifluoromethyl)phenyl)ethynyl)phenyl)-1-(4-methoxyphenyl)prop-2-yn-1-one (**16**).* Terminal alkyne **8** (0.093 g, 0.35 mmol) was rinsed into an argon-flushed storage tube with freshly distilled NEt_3 (20 mL). $Pd(PPh_3)_4$ (23.1 mg, 0.020 mmol), CuI (3.8 mg, 0.020 mmol), and 1-chloro-2-iodo-4-(trifluoromethyl)benzene (0.060 mL, 0.38 mmol) were added, and the tube was sealed and heated at 80 °C for 20 h. After cooling to room temperature, the mixture was rinsed into a separatory funnel with ethyl acetate. The organic layer was washed with NH_4Cl solution, dried with anhydrous Na_2SO_4, filtered, and concentrated. The crude residue was purified via flash chromatography using a solvent gradient (silica, 10% $CHCl_3$/90% hexane, increasing gradually to 75% $CHCl_3$/25% hexane), revealing alcohol intermediate **12** as a light brown oil (0.151 g, 0.34 mmol, 97% yield). ^{1}H NMR (400 MHz, $CDCl_3$): δ 7.79 (s, 1H), 7.58 (m, 1H), 7.55 (d, J = 8.8 Hz, 2H), 7.53 (m, 2H), 7.48 (dd, J = 8.5, 1.6 Hz), 7.33 (m, 2H), 6.79 (d, J = 8.7 Hz, 2H), 5.70 (d, J = 5.8 Hz, 1H), 3.75 (s, 3H), 2.33 (d, J = 6.0 Hz, 1H) ppm. ^{13}C NMR (100 MHz, $CDCl_3$) δ 159.7, 139.5, 132.7, 132.2, 130.3, 129.9, 129.4, 129.1, 128.9, 128.4, 128.2, 125.8, 125.3, 124.9, 124.1, 124.0 (q, J = 270 Hz), 113.9, 94.7, 93.4, 88.5, 84.8, 64.9, 55.2 ppm. APCI-QTOF (m/z) calcd for $C_{25}H_{15}ClF_3O_2^-$ 439.0713; found 439.0708. Intermediate alcohol **12** (0.151 g, 0.34 mmol) was dissolved in 20 mL dry CH_2Cl_2. Celite (0.75 g), 3 Å sieves (1.0 g), and PCC (86 mg, 0.40 mmol) were added, and the mixture was stirred for 1 day at room temperature. The entire reaction mixture was loaded onto a silica gel column, and the components were separated by gradually increasing the mobile phase from 50% hexane/50% $CHCl_3$ to 100% $CHCl_3$. The product was isolated as a white solid (0.111 g, 0.25 mmol, 74% yield). ^{1}H NMR (400 MHz, $CDCl_3$): δ 8.24 (d, J = 8.9 Hz, 2H), 7.82 (d, J = 1.6 Hz, 1H), 7.77 (dd, J = 7.6, 1.2 Hz, 1H), 7.67 (dd, J = 7.7, 1.0 Hz, 1H), 7.55 (d, J = 8.5 Hz, 1H), 7.51 (dd, J = 7.0, 2.0 Hz, 1H), 7.47 (td, J = 7.6, 1.6 Hz, 1H), 7.43 (td, J = 7.6, 1.6 Hz, 1H), 6.75 (d, J = 8.9 Hz, 2H), 3.79 (s, 3H) ppm. ^{13}C NMR (100 MHz, $CDCl_3$) δ 176.4, 164.5, 140.0, 133.6, 132.6, 132.1, 130.3 (q, J = 3.8 Hz), 130.28, 130.24, 130.0, 129.3 (q, J = 33.4 Hz), 129.1, 126.2 (q, J = 3.6 Hz), 126.1, 123.7, 123.3 (q, J = 271 Hz), 123.2, 113.7, 94.1, 90.5, 89.9, 89.5, 55.4 ppm. APCI-QTOF (m/z) calcd for $C_{25}H_{14}ClF_3O_2H^+$ 439.0713; found 439.0704.

dx.doi.org/10.1021/jo501015x | J. Org. Chem. 2014, 79, 6269−6278

*2-((2-((2-Bromo-3,4,5,6-tetrafluorophenyl)ethynyl)phenyl)-ethynyl)quinoline (**20**).* Terminal alkyne **19** (0.666 g, 2.63 mmol) was dissolved in dry THF (20 mL) and transferred to a storage tube under argon. After 5 mL NEt_3 was added, argon was bubbled through the mixture for 15 min. 1,2-Dibromotetrafluorobenzene (0.413 mL, 3.0 mmol), $Pd(PPh_3)_4$ (0.152 g, 0.13 mmol), and CuI (25 mg, 0.13 mmol) were added. The tube was sealed under argon and heated at 60 °C for 4 days. An off-white precipitate formed. After the mixture was cooled in an ice bath, this precipitate was isolated via suction filtration and rinsed with water, then hexane. Two crops of off-white solid were isolated totaling 235 mg (0.49 mmol, 19% yield) product. ^{1}H NMR (400 MHz, $CDCl_3$), very low solubility in NMR solvent: δ 8.16 (d, J = 8.6 Hz, 1H), 8.14 (d, J = 8.6 Hz, 1H), 7.83 (d, J = 8.2 Hz, 1H), 7.76 (m, 2H), 7.69 (m, 1H), 7.65 (d, J = 8.3 Hz, 1H), 7.58 (m, 1H), 7.43 (m, 2H) ppm. APCI-QTOF (m/z) calcd for $C_{25}H_{10}BrF_4NH^+$ 480.0011/481.9991; found 480.0016/481.9999.

*2-((2-((2,3,4,5-Tetrafluoro-6-iodophenyl)ethynyl)phenyl)ethynyl)-quinoline (**21**).* Terminal alkyne **19** (75 mg, 0.30 mmol) was rinsed into an air-free storage tube under argon with NEt_3 (20 mL). 1,2-Diiodotetrafluorobenzene (0.40 g, 1.00 mmol), $Pd(PPh_3)_4$ (10.4 mg, 0.009 mmol), and CuI (1.7 mg, 0.009 mmol) were added, and the tube was sealed under argon and heated at 80 °C for 22 h. After cooling to room temperature, NH_4Cl solution was added to the reaction tube. The contents were rinsed into a separatory funnel with $CHCl_3$. The layers were separated, and the organic layer was dried with anhydrous Na_2SO_4, filtered, and concentrated. Purification of this material via flash chromatography (silica, 100% $CHCl_3$) yielded the product as a white solid (74.4 mg, 0.14 mmol, 47% yield). ^{1}H NMR (400 MHz, $CDCl_3$), very low solubility in NMR solvent: δ 8.16 (d, J = 8.5 Hz, 1H), 8.13 (d, J = 8.6 Hz, 1H), 7.82 (d, J = 8.1 Hz, 1H), 7.76 (m, 2H), 7.70 (m, 1H), 7.66 (d, J = 8.4 Hz, 1H), 7.58 (m, 1H), 7.43 (m, 2H) ppm. ^{13}C NMR (100 MHz, $CDCl_3$) extensive fluorine coupling makes ^{13}C signals of fluorinated ring and neighboring alkyne impossible to accurately interpret at achievable concentrations, δ 148.0, 143.4, 136.3, 133.5, 133.1, 130.3, 129.4, 129.2, 129.0, 127.6, 127.4, 127.2, 125.1, 124.8, 124.7, 93.5, 89.5 ppm. ^{19}F NMR (376.4 MHz, $CDCl_3$) δ −114.6 (ddd, J = 23.2, 10.2, 3.5 Hz), −130.9 (ddd, J = 20.6, 10.5, 3.9 Hz), −151.5 (m), −154.8 (td, J = 19.9, 3.4 Hz) ppm. APCI-QTOF (m/z) calcd for $C_{25}H_{10}F_4INH^+$ 527.9872; found 527.9875.

■ ASSOCIATED CONTENT

Ⓢ Supporting Information

X-ray data in CIF format and ^{1}H/^{13}C spectra for **6**−**16** and **18**−**21**; Cartesian coordinates for calculated structures; and ellipsoid representations of X-ray data. This material is available free of charge via the Internet at http://pubs.acs.org.

■ AUTHOR INFORMATION

Corresponding Author

*E-mail: nbowling@uwsp.edu.

Notes

The authors declare no competing financial interest.

■ ACKNOWLEDGMENTS

The authors gratefully acknowledge that this material is based upon work supported by the National Science Foundation under grant CHE-1306284. The authors also acknowledge that NMR characterization was based upon work supported by the National Science Foundation under grant CHE-0957080. HRMS characterization was based upon work supported by the National Science Foundation under CBET-0958711. The Missouri State University Provost Incentive Fund funded the purchase of the X-ray diffractometer. Computational resources were provided by the Midwest Undergraduate Computational Chemistry Consortium (MU3C) through NSF-MRI CHE-1039925.

■ REFERENCES

(1) Desiraju, G. R.; Ho, P. S.; Kloo, L.; Legon, A. C.; Marquardt, R.; Metrangolo, P.; Politzer, P.; Resnati, G.; Rissanen, K. *Pure Appl. Chem.* **2013**, *85*, 1711.
(2) Murray, J. S.; Riley, K. E.; Politzer, P.; Clark, T. *Aust. J. Chem.* **2010**, *63*, 1598.
(3) Metrangolo, P.; Resnati, G. *Science* **2008**, *321*, 918.
(4) Metrangolo, P.; Neukirch, H.; Pilati, T.; Resnati, G. *Acc. Chem. Res.* **2005**, *38*, 386.
(5) Lommerse, J. P. M.; Stone, A. J.; Taylor, R.; Allen, F. H. *J. Am. Chem. Soc.* **1996**, *118*, 3108.
(6) Politzer, P.; Murray, J. S.; Clark, T. *Phys. Chem. Chem. Phys.* **2013**, *15*, 11178.
(7) Fourmigue, M. *Curr. Opin. Solid State Mater. Sci.* **2009**, *13*, 36.
(8) Scholfield, M. R.; Vander Zanden, C. M.; Carter, M.; Ho, P. S. *Protein Sci.* **2013**, *22*, 139.
(9) Auffinger, P.; Hays, F. A.; Westhof, E.; Ho, P. S. *Proc. Natl. Acad. Sci. U.S.A.* **2004**, *101*, 16789.
(10) Jorgensen, W. L.; Schyman, P. *J. Chem. Theory Comput.* **2012**, *8*, 3895.
(11) Wilcken, R.; Zimmermann, M. O.; Lange, A.; Joerger, A. C.; Boeckler, F. M. *J. Med. Chem.* **2013**, *56*, 1363.
(12) Meyer, F.; Dubois, P. *CrystEngComm* **2013**, *15*, 3058.
(13) Troff, R. W.; Makela, T.; Topic, F.; Valkonen, A.; Raatikainen, K.; Rissanen, K. *Eur. J. Org. Chem.* **2013**, 1617.
(14) Hardegger, L. A.; Kuhn, B.; Spinnler, B.; Anselm, L.; Ecabert, R.; Stihle, M.; Gsell, B.; Thoma, R.; Diez, J.; Benz, J.; Plancher, J. M.; Hartmann, G.; Banner, D. W.; Haap, W.; Diederich, F. *Angew. Chem., Int. Ed.* **2011**, *50*, 314.
(15) Lu, Y. X.; Wang, Y.; Zhu, W. L. *Phys. Chem. Chem. Phys.* **2010**, *12*, 4543.
(16) Xu, Z. J.; Yang, Z.; Liu, Y. T.; Lu, Y. X.; Chen, K. X.; Zhu, W. L. *J. Chem. Inf. Model* **2014**, *54*, 69.
(17) Metrangolo, P.; Carcenac, Y.; Lahtinen, M.; Pilati, T.; Rissanen, K.; Vij, A.; Resnati, G. *Science* **2009**, *323*, 1461.
(18) Priimagi, A.; Cavallo, G.; Metrangolo, P.; Resnati, G. *Acc. Chem. Res.* **2013**, *46*, 2686.
(19) Rissanen, K. *CrystEngComm* **2008**, *10*, 1107.
(20) Metrangolo, P.; Meyer, F.; Pilati, T.; Resnati, G.; Terraneo, G. *Angew. Chem., Int. Ed.* **2008**, *47*, 6114.
(21) Coulembier, O.; Meyer, F.; Dubois, P. *Polym. Chem.* **2010**, *1*, 434.
(22) Jungbauer, S. H.; Schindler, S.; Kniep, F.; Walter, S. M.; Rout, L.; Huber, S. M. *Synlett* **2013**, *24*, 2624.
(23) Sarwar, M. G.; Dragisic, B.; Dimitrijevic, E.; Taylor, M. S. *Chem.—Eur. J.* **2013**, *19*, 2050.
(24) Chudzinski, M. G.; McClary, C. A.; Taylor, M. S. *J. Am. Chem. Soc.* **2011**, *133*, 10559.
(25) Jentzsch, A. V.; Hennig, A.; Mareda, J.; Matile, S. *Acc. Chem. Res.* **2013**, *46*, 2791.
(26) Erdelyi, M. *Chem. Soc. Rev.* **2012**, *41*, 3547.
(27) Sarwar, M. G.; Dragisic, B.; Salsberg, L. J.; Gouliaras, C.; Taylor, M. S. *J. Am. Chem. Soc.* **2010**, *132*, 1646.
(28) Chudzinski, M. G.; Taylor, M. S. *J. Org. Chem.* **2012**, *77*, 3483.
(29) Hu, Y. Z.; Chamchoumis, C.; Grebowicz, J. S.; Thummel, R. P. *Inorg. Chem.* **2002**, *41*, 2296.
(30) Forni, A. *J. Phys. Chem. A* **2009**, *113*, 3403.
(31) Walsh, R. B.; Padgett, C. W.; Metrangolo, P.; Resnati, G.; Hanks, T. W.; Pennington, W. T. *Cryst. Growth Des.* **2001**, *1*, 165.
(32) Tsuzuki, S.; Wakisaka, A.; Ono, T.; Sonoda, T. *Chem.—Eur. J.* **2012**, *18*, 951.
(33) Riley, K. E.; Murray, J. S.; Fanfrlik, J.; Rezac, J.; Sola, R. J.; Concha, M. C.; Ramos, F. M.; Politzer, P. *J. Mol. Model.* **2011**, *17*, 3309.
(34) Prasang, C.; Whitwood, A. C.; Bruce, D. W. *Cryst. Growth Des.* **2009**, *9*, 5319.
(35) Hoffmann, M.; Bischoff, D.; Dahmann, G.; Klicic, J.; Schaenzle, G.; Wollin, S. L. M.; Convers-Reignier, S. G.; East, S. P.; Marlin, F. J.;

McCarthy, C.; Scott, J.; PCT Int. Appl. WO2013014060 A1, Jan 31, 2013.
(36) Riley, K. E.; Murray, J. S.; Politzer, P.; Concha, M. C.; Hobza, P. *J. Chem. Theory Comput.* **2009**, *5*, 155.
(37) Bondi, A. *J. Phys. Chem.* **1964**, *68*, 441.
(38) Riley, K. E.; Hobza, P. *Phys. Chem. Chem. Phys.* **2013**, *15*, 17742.
(39) Politzer, P.; Murray, J. S. *ChemPhysChem* **2013**, *14*, 278.
(40) *Apex2 Suite*; Bruker AXS Ltd.: Madison, WI, 2006.
(41) Sheldrick, G. M. *Acta Crystallogr. A* **2008**, *64*, 112.
(42) Atwood, J. L.; Barbour, L. J. *Cryst. Growth Des.* **2003**, *3*, 3.
(43) *Gaussian 09*, Revision B.01; Frisch, M. J.; Trucks, G. W.; Schlegel, H. B.; Scuseria, G. E.; Robb, M. A.; Cheeseman, J. R.; Scalmani, G.; Barone, V.; Mennucci, B.; Petersson, G. A.; Nakatsuji, H.; Caricato, M.; Li, X.; Hratchian, H. P.; Izmaylov, A. F.; Bloino, J.; Zheng, G.; Sonnenberg, J. L.; Hada, M.; Ehara, M.; Toyota, K.; Fukuda, R.; Hasegawa, J.; Ishida, M.; Nakajima, T.; Honda, Y.; Kitao, O.; Nakai, H.; Vreven, T.; Montgomery, J. A., Jr.; Peralta, J. E.; Ogliaro, F.; Bearpark, M.; Heyd, J. J.; Brothers, E.; Kudin, K. N.; Staroverov, V. N.; Kobayashi, R.; Normand, J.; Raghavachari, K.; Rendell, A.; Burant, J. C.; Iyengar, S. S.; Tomasi, J.; Cossi, M.; Rega, N.; Millam, N. J.; Klene, M.; Knox, J. E.; Cross, J. B.; Bakken, V.; Adamo, C.; Jaramillo, J.; Gomperts, R.; Stratmann, R. E.; Yazyev, O.; Austin, A. J.; Cammi, R.; Pomelli, C.; Ochterski, J. W.; Martin, R. L.; Morokuma, K.; Zakrzewski, V. G.; Voth, G. A.; Salvador, P.; Dannenberg, J. J.; Dapprich, S.; Daniels, A. D.; Farkas, Ö.; Foresman, J. B.; Ortiz, J. V.; Cioslowski, J.; Fox, D. J. Gaussian, Inc., Wallingford CT, 2009.
(44) Zhao, Y.; Truhlar, D. G. *Theor. Chem. Acc.* **2008**, *120*, 215.
(45) Kozuch, S.; Martin, J. M. L. *J. Chem. Theory Comput.* **2013**, *9*, 1918.
(46) Rassolov, V. A.; Ratner, M. A.; Pople, J. A.; Redfern, P. C.; Curtiss, L. A. *J. Comput. Chem.* **2001**, *22*, 976.
(47) Peterson, K. A.; Shepler, B. C.; Figgen, D.; Stoll, H. *J. Phys. Chem. A* **2006**, *110*, 13877.
(48) Ge, G. C.; Mo, D. L.; Ding, C. H.; Dai, L. X.; Hou, X. L. *Org. Lett.* **2012**, *14*, 5756.